ACS APPLIED MATERIALS & INTERFACES

Research Article

www.acsami.org

Polycation-*b*-Polyzwitterion Copolymer Grafted Luminescent Carbon Dots As a Multifunctional Platform for Serum-Resistant Gene Delivery and Bioimaging

Lu Cheng,[†,§] Yongmao Li,[†,§] Xinyun Zhai,[†] Bing Xu,[†] Zhiqiang Cao,[‡] and Wenguang Liu*[,†]

[†]School of Materials Science and Engineering, Tianjin Key Laboratory of Composite and Functional Materials, Tianjin University, Tianjin 300072, China

[‡]Department of Chemical Engineering and Materials Science, Wayne State University, Detroit, Michigan 48202, United States

Supporting Information

ABSTRACT: Nanomaterials that integrate functions of imaging and gene delivery have been of great interest due to their potential use in simultaneous diagnosis and therapy. Herein, polycation-*b*-polysulfobetaine block copolymer, poly[2-(dimethylamino) ethyl methacrylate]-*b*-poly[*N*-(3-(methacryloylamino) propyl)-*N*,*N*-dimethyl-*N*-(3-sulfopropyl) ammonium hydroxide] (PDMAEMA-*b*-PMPDSAH) grafted luminescent carbon dots (CDs) were prepared via surface-initiated atom transfer radical polymerization (ATRP) and investigated as a multifunctional gene delivery system (denoted as CD-PDMA-PMPD) in which the CD cores acted as good multicolor cell imaging probes, the cationic PDMAEMA acted as a DNA condensing agent, and the outer shell of zwitterionic PMPDSAH block protected the vector against nonspecific interactions with serum components. As revealed by the fluorescent spectrum study, the photoluminescent attributes, especially the tunable emission property, were well inherited from the parent CDs. The CD-PDMA-PMPD could condense plasmid DNA into nanospheres with sizes of approximate 50 nm at a proper complex ratio, posing little cytotoxicity at higher ratios. It was shown that the hybrid vector exhibited significantly suppressed BSA protein adsorption and superior hemocompatibility compared to those of the widely used PEI25k. In the in vitro transfection assay, an increased serum concentration from 10 to 50% caused a dramatic drop in PEI25k transfection performance, whereas the transfection efficiency of CD-PDMA-PMPD was well maintained; CD-PDMA80-PMPD40 showed 13 and 28 times higher transfection efficiencies than PEI25k at 30 and 50% serum concentration, respectively. Intriguingly, the carbon dots in the transfected cells displayed excitation-dependent fluorescent emissions, portending that this polycation-polyzwitterion modified CD will be a promising theranostic vector with excellent stealth performance.

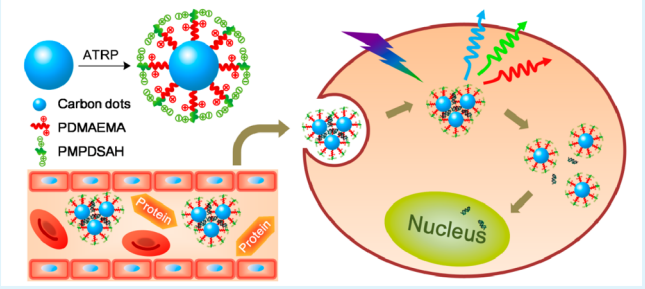

KEYWORDS: *carbon dots, polysulfobetaine, gene delivery, serum resistance, bioimaging*

1. INTRODUCTION

Combining nanosized chromophore and therapeutic agents, such as genes or drugs, holds great potential for versatile theranostics.[1,2] Fluorescent carbon dots (CDs) have recently drawn immense attention owing to their superiority in photostability, excitation-dependent emission tunability, flexibility in surface functionalization, easiness of preparation, remarkably low cytotoxicity, and excellent biocompatibility.[3] These novel nanoparticles are considered to be competitive alternatives to organic dyes and heavy metal based quantum dots (QDs), two prevalent agents for imaging that usually suffer from photobleaching and innate toxicity.[4,5] There has been significant research on CDs synthesis and their applications in bioimaging,[6−8] sensing,[9,10] photocatalysis,[11,12] optoelectronics,[13,14] drug delivery,[15−18] and so on. Among them, CD-based drug delivery systems have been developed based on particle surface modification, thanks to the numerous surface functional groups such as amino, hydroxyl and carboxyl. Tang et al. constructed a direct and sensitive Förster resonance energy transfer (FRET)-based CD drug delivery system (FRET-CDot-DDS) via EDC/NHS coupling protocol, which has shown excellent targeted delivery and drug release efficiency while achieving monitoring of the release process by recording the FRET efficiency between CDs and doxorubicin (DOX).[16] In a study by Zheng and co-workers, oxaliplatin conjugated CDs (CD-Oxa) were reported to exhibit both effective anticancer function and multicolor imaging ability for temporal and spatial detection of therapy.[17] Nevertheless, little research on CD-based gene delivery has been reported thus far.[19,20] We believe the combination of fluorescent CDs with gene delivery function is promising for

Received: September 6, 2014
Accepted: October 6, 2014
Published: October 6, 2014

real-time tracking of gene transfection and shedding light on transfection mechanisms.

Gene delivery carriers based on cationic polymers are historically preferred, given their advantages in encapsulating negatively charged DNA and facilitating desirable intracellular trafficking.[21] Nonetheless, their applications are greatly limited due to their lack of serum stability, rapid clearance in biological environment, and damage to cellular membranes caused by their nonspecific interactions with anionic components in blood and on cell membranes.[22] Hydrophilic and uncharged polymers such as poly(ethylene glycol) (PEG) are commonly employed to shield the surface of the polycation/DNA complexes via steric stabilization, resulting in reduced nonspecific protein adsorption and, in turn, prolonged circulation in blood.[23] Paradoxically, PEGylation can also bring a steric hindrance that hampers the efficient interaction between DNA complexes and celluar membranes, thus deteriorating the transfection efficiency.[24] To this end, several strategies including the conjugation with neutral and anionic liposomes have also been developed.[25] Lately, zwitterionic polymers such as polyphosphorylcholine, polysulfobetaine, and polycarboxybetaine have been proved to be promising alternatives to PEG due to their ultrahigh resistance to nonspecific protein adsorption,[26,27] holding the potential for the construction of serum-resistant nonviral gene vectors.[28−30] Our previous study demonstrated that polycation-*b*-polysulfobetaine diblock copolymer, poly[2-(dimethylamino) ethyl methacrylate]-*b*-poly[*N*-(3-(methacryloylamino) propyl)-*N*,*N*-dimethyl-*N*-(3-sulfopropyl) ammonium hydroxide] (PDMAEMA-*b*-PMPDSAH) exhibited increased gene transfection efficiency at higher serum concentrations compared to that of PDMAEMA homopolymer.[28] The polysulfobetaine segment was shown to promote the endocytosis of nanocomplexes while maintaining a high serum-resistant ability. However, the copolymer exhibited inferior transfection efficiency to that of PEI25k at 10% serum and only limited increase compared with PEI25k at higher serum concentrations due to its linear structure.

To extend this polyzwitterion to theranostics, we developed PDMAEMA-*b*-PMPDSAH block-copolymer-coated CDs and demonstrated perfect integration of bioimaging capability with a serum-resistant gene delivery function. Surface-initiated atom transfer radical polymerization (ATRP), which has seldom been employed in CD modification, was used to prepare the polymer-coated CDs. The physicochemical properties, biocompatibility, and hemocompatibility of the CD-polymers were investigated, and transfection experiments at various serum concentrations were conducted. It was found that zwitterionic PMPDSAH significantly increased the transfection capability of CD-polymers, even in the presence of a high concentration of serum. Also, by using laser scanning confocal microscopy, the multicolor cell imaging capacity of the CD-polymer was evaluated.

2. EXPERIMENTAL SECTION

2.1. Synthesis of PDMAEMA-*b*-PMPDSAH Copolymer Grafted Carbon Dots. *2.1.1. Preparation of Carbon Dots (CDs).* Luminescent carbon dots were prepared via a facile one-step microwave pyrolysis method as reported in our previous work.[31] Briefly, 2 g (10.41 mmol) of citric acid (CA) was dissolved in 20 mL double-deionized water in a common 100 mL beaker, followed by the addition of 1.04 mL (15.62 mmol) of 1,2-ethylenediamine (EDA) under vigorous stirring to form a clear, transparent solution. The beaker was subsequently placed at the center of the rotation plate of a domestic microwave oven (700 W) and heated for 4 min until the solution changed from colorless to yellow and finally red-brown. After cooling down to room temperature, the resultant was redissolved in pure water, dialyzed (MWCO of 500) for 3 days, and then lyophilized to collect dry CD solid.

2.1.2. Synthesis of Carbon Dot Initiator (CD-Br). CD-Br was synthesized through carbodiimide-assisted conjugation. First, 2 g (12.33 mmol) *N*,*N*′-carbonyldiimidazole (CDI) was added to 10 mL DMSO solution of 2.06 g (12.33 mmol) 2-bromoisobutyric acid (BiBA). After 3 h of stirring to allow for sufficient activation, 1 g of CDs dispersed in 10 mL of DMSO, which had undergone sonification for 1 h, was added to the mixture, and the new mixture was stirred for another 24 h at room temperature. The resultant CD-Br was precipitated with excess amount of THF. Then, the sediment was redissolved and dialyzed (MWCO of 500) against deionized water for 3 days. After subsequent lyophilization, the yellow-brown CD-Br powder was obtained.

2.1.3. Synthesis of PDMAEMA-b-PMPDSAH Copolymer Grafted Carbon Dots (CD-PDMA-PMPD). CD-polymer composites were fabricated via ATRP reaction, as described below. For CD-PDMA80, a 4 mL ethanol suspension of 2.5 mg (0.025 mmol) of CuCl was placed in a clean, dry Schlenk tube and degassed by three freeze−pump−thaw cycles. Then, 21.93 mg of CD-Br (containing 0.025 mmol Br), 340 μL (2 mmol) of DMAEMA, 5.22 μL (0.025 mmol) of *N*,*N*,*N*′,*N*″,*N*″- pentamethyldiethylenetriamine (PMDETA), and 2.922 mg (0.05 mmol) of NaCl dissolved in 5 mL of double-deionized water were added under N_2 protection. After another three freeze−pump−thaw cycles, the mixture was stirred for 3 h at room temperature. To synthesize CD-PDMA-PMPD, the reaction content was frozen, and 1 mL of water solution of 146.2 mg (0.5 mmol) or 292.4 mg (1 mmol) of MPDSAH was injected to the tube to obtain CD-PDMA80-PMPD20 or CD-PDMA80-PMPD40, respectively. The mixture was further degassed using the freeze−thaw method, and the reaction was performed at room temperature for 24 h. Finally, the reaction solution was dialyzed (MWCO of 3500) against deionized water for 7 days to completely remove the impurities and thereupon freeze-dried to collect anhydrous CD-polymers.

2.2. Preparation of CD-Polymer/pDNA Complexes. All the CD-polymer/pDNA complexes were freshly prepared before use. CD-polymers were dissolved in ultrapure water, and the solutions were subsequently sterilized by filtration via a 0.22 μm filter. The complexes of various ratios of particle/pDNA were obtained by dropping CD-polymer of appropriate concentrations to an equal volume of pDNA solution with defined concentration. The resulting mixture was gently vortexed and incubated for 30 min at room temperature to ensure complete complex formation. The complexing ratio was defined by the weight ratio of particle/pDNA.

2.3. DNase I Protection Assay. First, 5 μL of solutions of CD-polymer/pDNA complexes at desired weight ratios containing 0.5 μg pDNA were incubated with 4 μL of 10 × reaction buffer (20 mM Tris-HCl, 20 mM $MgCl_2$, pH 8.3) containing 0.1 U DNase I at 37 °C for 0, 30, 60, and 120 min. Three μL of 200 mM EDTA solution was added to terminate the digestion, followed by heat denaturation of DNase I at 70 °C for 10 min. The samples were subsequently treated with 15 μL of 10 mg/mL heparin solution under 60 °C for 3 h, resulting in pDNA dissociation from the complexes. The remaining pDNA was analyzed by agarose gel electrophoresis.

2.4. Hemolytic Activity Test. Whole rabbit blood was freshly collected and diluted five times with sterile PBS (pH = 7.4). Polymer samples at concentrations of 0.5 and 1.0 mg/mL were prepared in PBS (pH = 7.4) solution. Thereafter, the diluted blood (200 μL) was added into the polymer solution (800 μL), pipeting up and down to result in homogeneous mixing. Then, 800 μL of PBS solution and TritonX-100 solution (1% v/v) were used to replace the polymer solutions as negative and positive controls, respectively. The mixture was kept at 37 °C for 90 min and then centrifuged at 2000 rpm for 10 min. The supernatant (200 μL) was transferred to a 96-well plate where the absorbance at 543 nm was recorded on a Synergy HT Multi-Mode Microplate Reader (BioTek, USA). The hemolytic rate was calculated using the following formula:

Scheme 1. Synthetic Route of CDs, CD-Br, and CD-Polymers

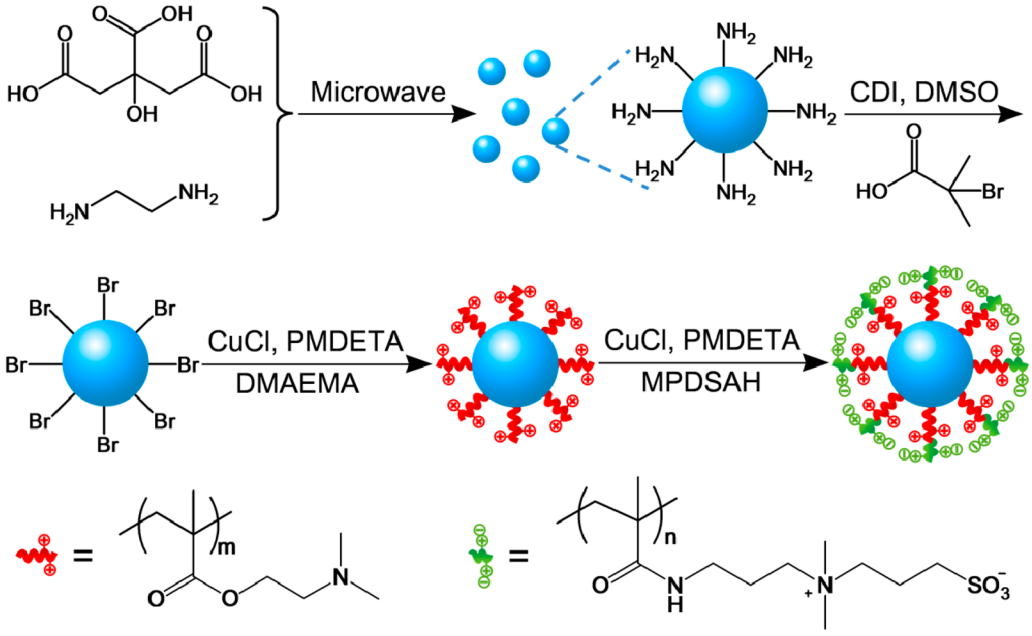

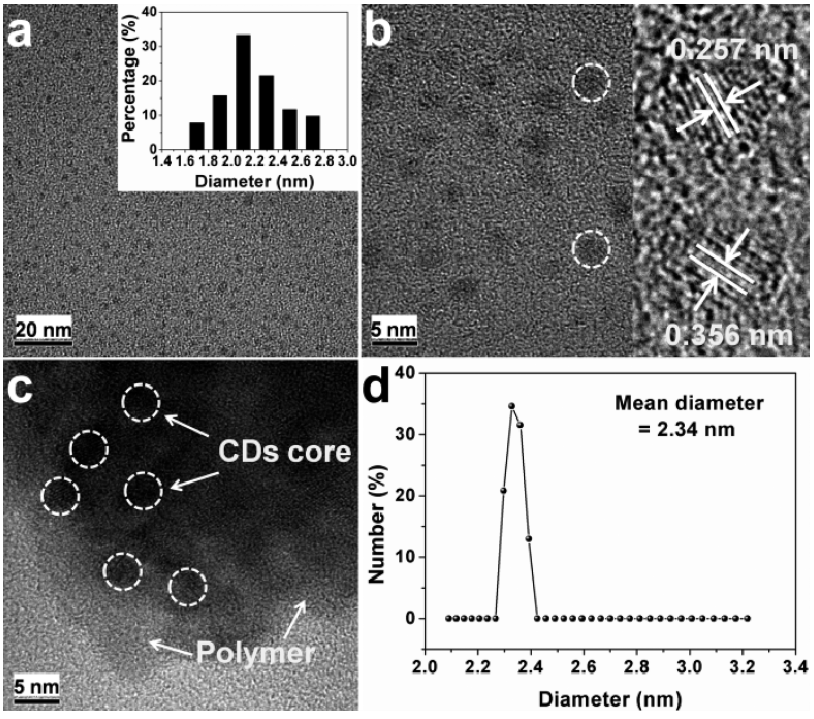

Figure 1. HRTEM images of (a and b) CDs and (c) CD-PDMA80-PMPD40. (d) DLS distribution plot of the diameter of CDs. Insets: (a) size distribution of CDs according to HRTEM; (b) typical single CDs and their lattice spacings. Scale bars: (a) 20 nm and (b and c) 5 nm.

$$\text{hemolytic rate} = \frac{A_s - A_n}{A_p - A_n} \times 100\%$$

where A_s, A_n and A_p represent the absorbance of sample, negative and positive controls, respectively.

2.5. Red Blood Cell Aggregation. Red blood cells were collected by centrifugation of fresh rabbit blood at 700 rpm for 10 min and then diluted with PBS (pH = 7.4) at 1:10 ratio. Then, 200 μL of the diluents containing CD-polymer/pDNA complexes at prescribed complexing ratios achieving the maximum transfection efficiency were seeded in a 24-well plate and incubated at 37 °C for 1 h. Aggregation was visualized on a 1X-51 inverted fluorescence microscope (Olympus, Japan) under bright field.

2.6. Cell Culture. COS-7 cells (African green monkey kidney cells) were obtained from Peking Union Medical College (Beijing, China) and cultured in Dulbecco's modified Eagle medium (DMEM, HyClone) with high glucose, containing 10% fetal bovine serum (FBS), 100 U/mL penicillin, and 100 mg/mL streptomycin at 37 °C in 5% CO_2 humidified atmosphere.

2.7. In Vitro Transfection Assay. COS-7 cells were seeded at a density of 5 × 10^4 cells/well in 24-well plates containing 500 μL of DMEM with 10% FBS in each well and incubated for 24 h at 37 °C in

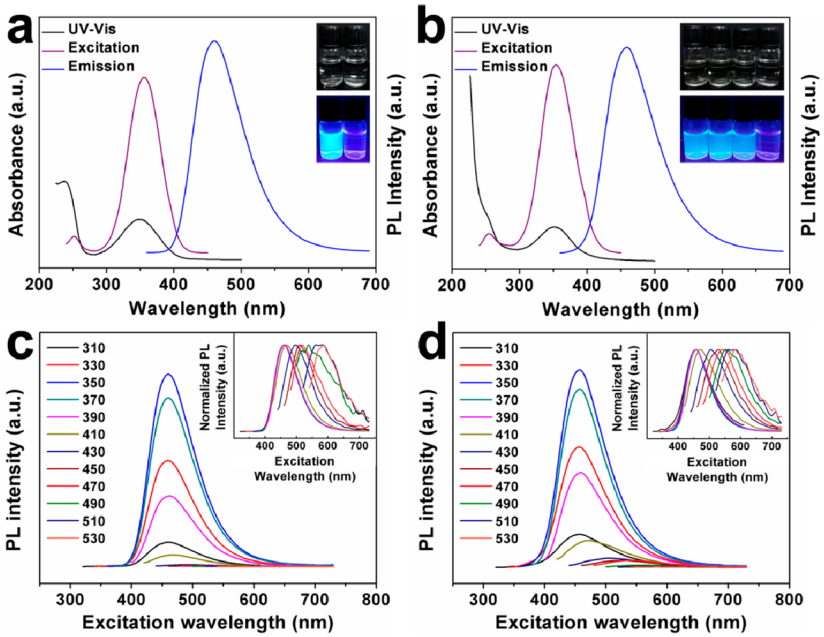

Figure 2. (a and b) UV−vis spectra and the maximum PL excitation and emission spectra of CDs and CD-PDMA80-PMPD40 in water, respectively. Insets: (upper) images of CDs and CD-polymers excited by daylight and (lower) UV; from left to right, (a) CDs and water, (b) CD-PDMA80, CD-PDMA80-PMPD20, CD-PDMA80-PMPD40, and water; the corresponding spectra of CD-PDMA80 and CD-PDMA80-PMPD20 are presented in Figure S9 (Supporting Information). (c and d) PL emission spectra of CDs and CD-PDMA80-PMPD40 aqueous solutions under different wavelength excitations, respectively. Insets: normalized PL intensity.

5% CO_2 humidified atmosphere. The medium was replaced with 450 μL of fresh medium with 10, 30, or 50% FBS. Particle/pDNA complexes (50 μL, containing 1 μg pDNA) at various weight ratios were then added to each well (n = 3 for each ratio). After 4 h of incubation at 37 °C in 5% CO_2, the transfection medium was aspirated and replaced with 500 μL of 10% FBS containing fresh medium. The transfected cells were incubated for an additional 48 h. Following incubation, the culture medium was discarded, and each well was rinsed twice with PBS. The cells in each well were treated with 150 μL of 1 × reporter lysis buffer (RLB, Promega) for 15 min followed by a freeze−thaw cycle to ensure complete lysis. The lysate was centrifuged for 5 min at 13 000 rpm; then, the supernatant was collected, and the luciferase activity was measured according to the standard protocols of Bright-Glo luciferase assay system (Promega, USA). The total protein was measured with a BCA protein assay kit (Pierce, USA), and the results were expressed in terms of relative light units (RLU) per milligram cell protein. For pEGFP-C1 plasmid transfection experiment in COS-7 cells, the transfected cells were observed on an inverted fluorescence microscope (Olympus 1X-51, Japan). Cells transfected with PEI25k were used as a positive control at a weight ratio of 2:1.

2.8. Cellular Uptake of CD-Polymer/pDNA Complexes. To investigate the cellular uptake capacity of the CD-polymer/pDNA complexes, pGL3-control was first labeled with fluorescent dye YOYO-1. Briefly, 1 mmol/L YOYO-1 was diluted 100 times in PBS. Next, 100 μg of pDNA was mixed with 100 μL of YOYO-1 dilution (1 molecule of YOYO-1 per 152 base pairs of pDNA) and incubated for 2 h in the dark. Then, the labeled pDNA was blended with the particles to form complexes. COS-7 cells, seeded at a density of 4×10^5 cells/well in 6-well plates and grown for 24 h, were incubated for another 4 h after replacing the medium with 1800 μL of DMEM with different concentrations of FBS without antibiotics and 200 μL of complex solution containing 6 μg pDNA. Finally, the cells were washed with cold PBS to remove the noninternalized complexes, trypsinized, and harvested in PBS. The fluorescence intensity and distribution of the cells were measured by flow cytometry using a FACSCalibur flow cytometer (BD, USA) equipped with an argon ion laser (488 nm emission wavelength), and the fluorescence was detected with a 530 ± 30 nm band-pass filter (FL1). Data acquisition was performed in linear mode, and data were visualized in logarithmic mode. For each sample, 1×10^4 events were collected. Data were analyzed using CellQuest software, and appropriate gating was applied to the scatterplots. The final results were expressed as cell counts versus FL1-H fluorescence intensity.

2.9. Statistical Analysis. Group data are reported as mean ± standard deviation (SD). For transfection results, the Student's t test was used to determine whether data groups are significantly different from each other. Statistical significance was defined as having $P < 0.05$.

3. RESULTS AND DISCUSSION

3.1. Characterization of CDs, CD-Br, and CD-Polymers. The synthetic route of CDs, CD-Br, and CD-polymers is illustrated in Scheme 1. First, highly luminescent CDs were prepared through one-pot microwave-assisted pyrolysis of CA in the presence of EDA passivator, a procedure we previously developed.[31] These carbon nanodots are uniformly dispersed spherical particles with an ultrasmall size of 2.2 ± 0.3 nm, as determined from the high-resolution transmission electron microscopy (HRTEM) image (Figure 1a). This particle size is also confirmed by dynamic light scattering (DLS; Figure 1d), suggesting an average hydrodynamic diameter of 2.3 nm. Further magnified HRTEM images showed well-resolved lattice fringes with widths of 0.257 and 0.356 nm attributed to the (020) and (002) planes of graphitic carbon, respectively.[16] The FTIR spectrum of the CDs shows a broad peak centered at 3396 cm^{-1} and extending across a large wavelength range (Figure S3, Supporting Information), suggesting the existence of −OH and especially $-NH_2$, which formed the basis of subsequent surface functionalization. Moreover, the X-ray photoelectron spectroscopy (XPS) analysis reveals that the CDs are mainly composed of C, N, and O elements (Figure S4a, Supporting Information), and the fitted high-resolution spectra further prove that there are C−N, C−O, C═O, and N−H bonds in the CDs (Figure S5a,c,e Supporting Information).

Table 1. Calculated Polymer Chain Lengths and Molecular Weights of CD-Polymers

	theoretical length		actual length[a]			
sample	DMA (p)	MPD (q)	DMA (m)	MPD (n)	molecular weight per chain	molecular weight[b]
CD-DMA80	80		67		10533	56488
CD-DMA80-MPD20	80	20	67	15	14919	80011
CD-DMA80-MPD40	80	40	67	32	19890	106670

[a]Calculated from integration of peaks in the ^{1}H NMR spectra. [b]Calculated by multiplying the molecular weight per chain by the estimated number of initiators on each CD-Br.

Photoluminescence is the most fascinating property of CDs among other carbon nanomaterials. The UV−vis spectrum of the CDs shows a broad absorption peak at 350 nm (with an absorption coefficient of 7.3 L/(g cm) according to Lambert−Beer's Law) and another at 245 nm (Figure 2a), which is typical for the $\pi-\pi^*$ transition of the C═C structures.[32] Upon excitation of the CDs aqueous solution with the optimal excitation wavelength at 350 nm, bright blue fluorescence centered at 460 nm could be observed (inset of Figure 2a). The quantum yield (QY) of the synthesized CDs at 350 nm excitation was calculated to be 41.5%, using quinine sulfate (QY = 54%) as a standard and following the reported method.[19] A single fluorescence lifetime of 15.87 ns was obtained under the same excitation conditions (Figure S6, Supporting Information). The CDs exhibit excitation-wavelength-dependent photoluminescent behavior, which is a common phenomenon for CDs.[3] With the excitation wavelength increasing from 310 to 530 nm, the emission peak red-shifted from 455 to 600 nm (Figure 2c). The QY of the CDs changed to 10.1% at 530 nm excitation using rhodamine B (QY = 97% in ethanol solution) as a standard. In addition, a drop of the CD solution was observed to exhibit blue, green, and red luminescence under ultraviolet (330−385 nm), blue (460−495 nm), and green (530−550 nm) light excitation, respectively, under a fluorescent microscope (Figure S7a, Supporting Information).

The ATRP initiator CD-Br was synthesized by amidation reaction mediated by the coupling agent CDI. Conjugation of BiBA on the CDs was confirmed by the appearance of the peak at 1.73 ppm compared to CDs in ^{1}H NMR spectrum (Figure S8a,b, Supporting Information), which is the feature signal of $-NH-CO-C(Br)-(CH_3)_2$, and the new peaks centered at 187.5 and 69.5 eV correspond to the Br 3p and Br 3d binding energies, respectively, in the XPS spectrum (Figure S4b, Supporting Information). The content of Br in CD-Br was determined by elemental analysis, showing a mass fraction of 9.12%.

Surface-initiated ATRP was utilized to synthesize the PDMA-*b*-PMPD copolymer-brush-modified CDs. Figure 1c shows the typical HRTEM image of the resulting CD-polymer. Unlike that of the parent CDs, the nanostructure of the single CD can hardly be identified due to the shielding of the polymer chains. Nevertheless, the core/shell structure of the CD-polymer can be recognized. DLS was used to measure the hydrodynamic size of the CD-polymers (Table S1, Supporting Information), showing 24.8 ± 1.6, 31.9 ± 2.0, and 38.4 ± 2.1 nm for CD-PDMA80, CD-PDMA80-PMPD20 and CD-PDMA80-PMPD40, respectively. Due to the hydration effect of the polymer chains in water, the CD-polymers are much larger than the original CDs (about 2.3 nm), which are relatively rigid nanospheres. Photoluminescent measurements of CD-polymers were carried out to investigate the influence of the polymer shells on the fluorescent properties of the CDs. As shown in Figures 2b and S9a,b (Supporting Information), the maximum excitation and emission wavelengths remained unchanged (i.e., 350 and 460 nm, respectively) after polymerization, and the absorption peak at about 350 nm was well retained. There was a stronger absorption in the far-UV region due to the absorbing character of the polymers. The resulting CD-polymers also had excitation-dependent fluorescent property similar to the parent CDs (Figures 2d and S9c,d, Supporting Information) exhibiting blue, green, and red emissions under the excitation of different color lights (Figure S7b, Supporting Information). The QYs of CD-PDMA80, CD-PDMA80-PMPD20, and CD-PDMA80-PMPD40 were 15.9, 14.3, and 13.7% at 350 nm excitation, and decreased to 4.0, 3.7, and 3.5%, respectively, when excited by 530 nm light. These QYs were lower than the QY of parent CDs yet high enough for bioimaging. Previously, we showed that EDA played dual roles in improving the fluorescent performance of the CDs, that is, acting as the precursor for N-doping and bringing about the $-NH_2$ surface passivation.[31] We believe that the consumption of some $-NH_2$ during the particle surface modification was responsible for the decreased QY, while the doping N atoms remained unaffected.

^{1}H NMR spectra for CD-PDMA and CD-PDMA-PMPD (Figure S8c,d, Supporting Information) showed feature signals of DMA ($-N-(CH_3)_2$, δ = 2.3; $-CH_2-N-$, δ = 2.7; $-N-CH_2-CH_2-$, δ = 4.1; $-CH_2-$ (main chain), δ = 1.9; $-C-CH_3$, δ = 0.8) and MPD (SO_3-CH_2-, δ = 2.9; $SO_3-CH_2-CH_2-$, δ = 2.1; $SO_3-CH_2-CH_2-CH_2-$, δ = 3.4; $-(CH_3)_2$, δ = 3.0; $-NH-CH_2-$, δ = 3.3; $-NH-CH_2-CH_2-$, δ = 2.1; $-NH-CH_2-CH_2-CH_2$, δ = 3.3; $-CH_2-$ (main chain), δ = 1.9; $-C-CH_3$, δ = 0.8),[28] indicating the polymerization of the two segments. Additionally, FTIR spectra confirm the fabrication of CD-Br and CD-polymers (Figure S3, Supporting Information).

It is difficult to measure the molecular weight of polymer coatings on a particle through conventional methods, such as by gel permeation chromatography (GPC). Here, the ^{1}H NMR spectra are employed to estimate the molecular weights of the polymer chains (see Supporting Information). The loading density (LD) of the ATRP initiators on the surface of the CDs, and the number of Br initiating points, also the number of polymer chains, on each CD (n_{Br}) are assessed according to the equations below:[33]

$$\mathrm{LD} = \frac{N_{Br} N_A}{\frac{S_{CD}}{\rho_{CD} V_{CD}}}$$

$$n_{Br} = S_{CD} \times \mathrm{LD}$$

where N_{Br} is the number of Br moles in 1 g CD-Br (1.14 mmol/g, calculated from the weight percentage of Br, 9.12%, as mentioned above); N_A is Avogadro's number; S_{CD} and V_{CD} are the surface area and volume of one CD (calculated from the average diameter of 2.2 nm), respectively, and ρ_{CD} is the density of the CDs (1.44 g/cm^3, measured by pycnometer method using cyclohexane as the nonsolvent).

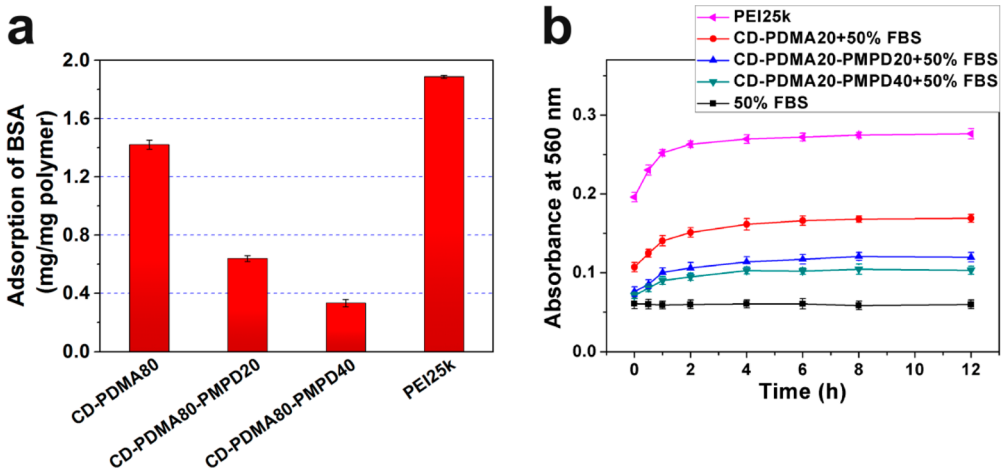

Figure 3. (a) BSA adsorption of CD-polymers and PEI25k. (b) Stability of CD-polymers and PEI25k in 50% FBS after coincubation for different time intervals. Results are presented as the mean ± SD, n = 3.

LD was calculated to be 0.359 initiator/nm^2, and the corresponding n_{Br} was 5.3 initiators/CD. The degree of polymerization of each polymer chain and the molecular weights of the CD-polymers are summarized in Table 1.

3.2. Formation of CD-Polymer/pDNA Complexes. Agarose gel electrophoresis was used to investigate the ability of the CD-polymers to condense pDNA, which is a crucial factor for efficient cell transfection. For all three polyplexes tested, their migrating ability in the gel decreased with increasing complexing ratio (Figure S11, Supporting Information). The complete retardation (full DNA condensation) was achieved at weight ratios of 0.8, 1.0, and 1.2 for CD-PDMA80, CD-PDMA80-PMPD20, and CD-PDMA80-PMPD40, respectively. Particles with longer PMPD chain length required more of them to fully condense the DNA due to the decreased cationic PDMA content and the charge shielding effect of PMPD (containing zwitterions).[28]

Zeta potential of the CD-polymer/pDNA at different weight ratios was measured to characterize the surface charges of the polyplexes. As shown in Figure S12a (Supporting Information), the zeta potentials of the three complexes are in the order of CD-PDMA80/pDNA > CD-PDMA80-PMPD20/pDNA > CD-PDMA80-PMPD40/pDNA at each selected weight ratio, suggesting correspondingly decreased ability to condense pDNA; this is consistent with the result of electrophoresis. As the complexing ratio increased, the zeta potential also increased and eventually reached over 30 mV. This will increase the affinity of complexes to negatively charged cell membrane surfaces, thereby facilitating the cellular uptake of nanoplexes.[34]

CD-polymers can effectively condense pDNA into nanosized spherical particles (about 50 nm), as revealed by the TEM images (Figure S13, Supporting Information). The average diameters of the CD-polymer/pDNA complexes determined by DLS showed a declining trend upon increasing the complexing ratio (Figure S12b, Supporting Information), and the results for the three polyplexes are in the order of CD-PDMA80/pDNA < CD-PDMA80-PMPD20/pDNA < CD-PDMA80-PMPD40/pDNA at each weight ratio. The higher surface charge density is responsible for the stronger condensation ability of CD-PDMA80, among others. Typically, the hydrodynamic diameters of the complexes (between 90 and 110 nm) measured by DLS are larger than those observed by TEM due to the hydration effect in aqueous solution at DLS condition. Moreover, all of the CD-polymers can well protect pDNA from enzymolysis (Figure S14, Supporting Information), which is another key criterion for gene vectors.

3.3. Protein Adsorption of CD-PDMA-PMPD. With respect to biomedical applications, protein adsorption onto the surface of biomaterials can usually cause serious inflammatory response, leading to platelet adhesion and thrombosis.[26] For gene delivery, the transfection efficiency is significantly compromised in the presence of serum for many cationic polymer vectors due to their nonspecific interactions with blood components.[35] Herein, BSA was selected as a model protein to simulate the blood albumin-rich conditions and determine the interactions between the CD-polymers and proteins. The BSA adsorbed by PEI25k and CD-PDMA80 exceeded 1.4 mg/mg polymer (Figure 3a), which was induced by electrostatic interactions between the negatively charged BSA and the highly positively charged polymers. By introducing PMPD blocks, the adsorption value dramatically drops to less than half of that for CD-PDMA80 or even about one-fourth, demonstrating the effective suppression of protein adsorption due to the introduction of zwitterionic PMPD block, which can shield the positive charges to some extent. A similar result is obtained when coincubating the vectors with 50% FBS. As shown in Figure 3b, CD-PDMA80-PMPD20 and CD-PDMA80-PMPD40 groups exhibit much lower absorbance than PEI25k and CD-PDMA80, which is due to the suppressed protein adsorption and thus decreased turbidity of the solutions. These results are consistent with the previous report that zwtterionic polymers have excellent ability to resist nonspecific protein adsorption.[26]

3.4. Blood Compatibility Assay. Blood compatibility is another important criterion for gene delivery systems to ensure their safe administration into the systemic circulation. The hemocompatibility of the CD-polymers was assessed by both hemolysis and red blood cell aggregation tests. Visual observation of hemolysis caused by the polymers is shown in Figure 4a. As shown in Figure 4b, PEI25k was found to cause more serious hemolysis (43.5 and 54.6% at 0.5 and 1 mg/mL polymer concentrations, respectively). The high hemolytic damage rate of PEI25k is attributable to its excessively strong electrostatic interaction with membrane proteins and phospholipids, which results in disturbed membrane structure and function.[36] CD-PDMA80 caused over 10% hemolysis at the

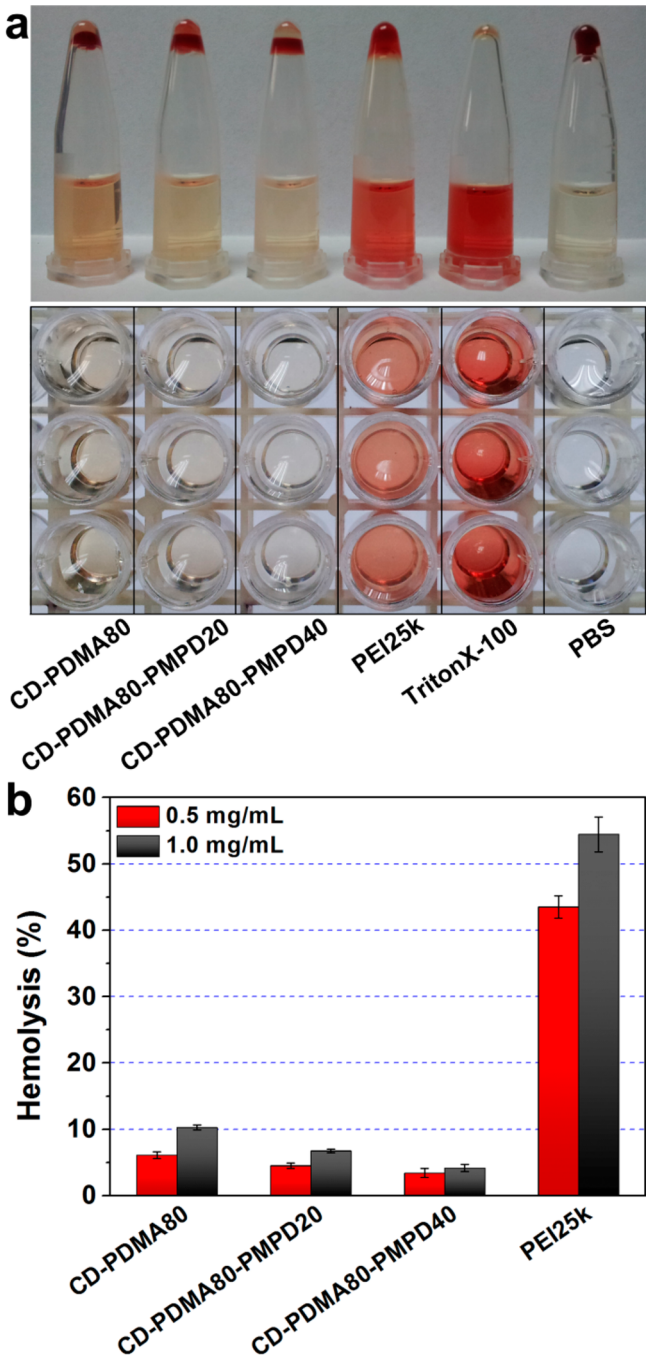

Figure 4. (a) Visual observation of the hemolysis caused by CD-polymers and PEI25k in phosphate buffer solution at pH 7.4 with TritonX-100 and PBS as positive and negative control, respectively. (b) Hemolytic rates of CD-polymers and PEI25k at concentrations of 0.5 and 1.0 mg/mL. Results are presented as the mean ± SD, n = 3.

concentration of 1.0 mg/mL, while CD-PDMA80-PMPD20 (at 0.5 mg/mL) and CD-PDMA80-PMPD40 (at both 0.5 and 1.0 mg/mL) displayed hemolysis rates of lower than 5%, which can be considered to elicit little to no hemolytic reaction.[37] The zwitterionic polymer modified CDs exhibit superior hemolysis-resistance performance to the crude CDs or carbon nanoparticles derived from spider silk, sucrose, glycine,[38−40] and even PEG-modified CDs.[8]

In addition to hemolysis, the absence of hemagglutination is regarded as another main criterion for blood compatibility since undesirable red blood cell (RBC) aggregation can induce serious circulatory disorders and even lethal toxicity.[41] Figure 5

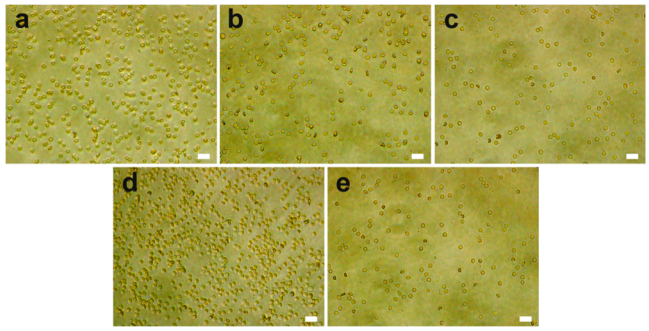

Figure 5. Micrographs of red blood cells after incubation with polyplexes of (a) CD-PDMA80/pDNA (16:1 w/w), (b) CD-PDMA80-PMPD20/pDNA (20:1 w/w), (c) CD-PDMA80-PMPD40/pDNA (24:1 w/w), (d) PEI25k/pDNA (2:1 w/w), and (e) PBS. Scale bars: 20 μm.

shows the effect of the CD-polymer/pDNA and PEI25k/pDNA complexes on the aggregation of RBC at the selected weight ratios. Serious and slight RBC aggregation was observed for PEI25k/pDNA and CD-PDMA80/pDNA, respectively, while for CD-PDMA-PMPD, only negligible aggregation was detected. Both hemolysis and RBC aggregation tests demonstrate that the CD-PDMA-PMPD (modified with zwitterionic polymers) is highly hemocompatible.

3.5. Cytotoxicity Evaluation of the CD-Polymers. Low toxicity and great biocompatibility are generally prominent characteristics for carbon dots, while cationic vectors usually show relatively greater toxicity to the cultured cells. To investigate the cytotoxicity of the polymer integrated CDs, in vitro MTT assay was carried out for CD-PDMA80/pDNA, CD-PDMA80-PMPD20/pDNA, and CD-PDMA80-PMPD40/pDNA complexes in COS-7 cells. From the results displayed in Figure S15 (Supporting Information), it is seen that all the samples exhibit a complex ratio-dependent cytotoxicity, with higher amount of CD-polymers in the complexes leading to lower cell viability. Importantly, zwitterionic PMPD modified particles showed less cytotoxicity than nonzwitterionic modified particles (Figure S15, Supporting Information). It is well accepted that particles with high positive charge density can cause damage to cell membranes and induce cytotoxicity. The introduction of zwitterionic PMPD blocks can lessen the damage effect due to its charge shielding property.

3.6. In Vitro Gene Transfection. The in vitro transfection activities of the CD-polymers were investigated in COS-7 cells using pGL-3 and pEGFP-C1 plasmids as reporter genes, respectively. The transfection efficiencies of the three CD-polymer/pDNA complexes at various weight ratios in the presence of different concentrations of serum for the luciferase assay are shown in Figure 6a−c. The optimal transfection efficiencies were achieved at 16:1, 20:1, and 24:1 for CD-PDMA80, CD-PDMA80-PMPD20, and CD-PDMA80-PMPD40, and they are 2.0, 3.0, and 3.6-fold that of PEI25k at 10% serum concentration, respectively. The higher transfection efficiencies of the CD-polymers at 10% serum compared with PEI25k were probably due to the star-shaped structures, which have been reported to enhance the performance of polycation gene vectors.[42]

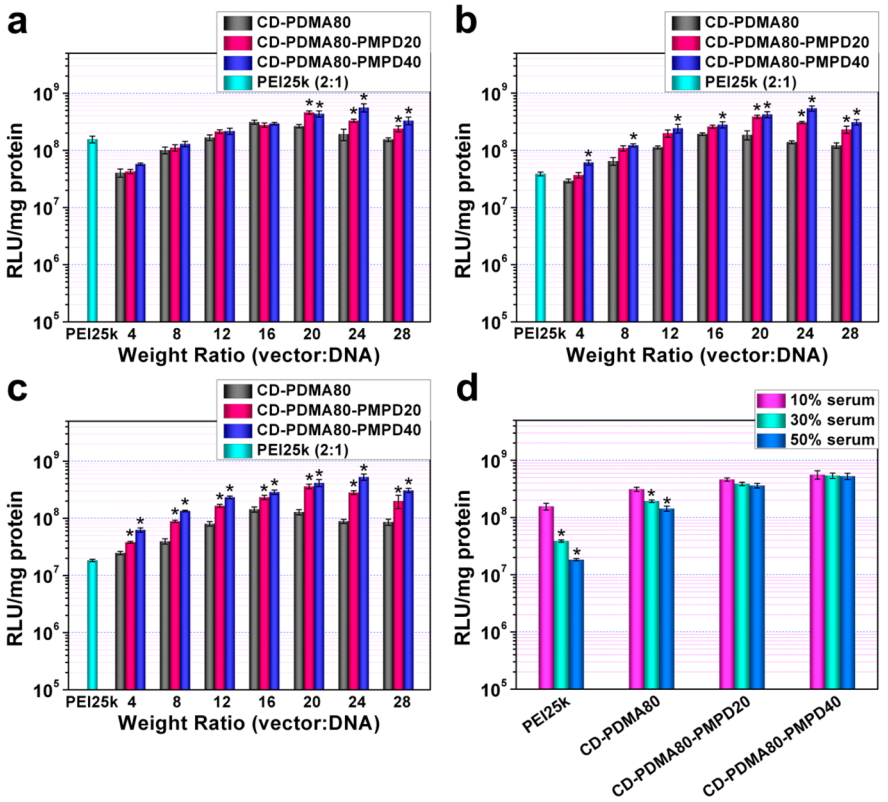

Figure 6. In vitro luciferase gene transfection efficiency of CD-polymers/pDNA complexes at varied weight ratios relative to that of PEI25k/pDNA in the presence of (a) 10, (b) 30, and (c) 50% serum concentrations in COS-7 cells. (d) Comparison of transfection performances of PEI25k/pDNA, CD-PDMA80/pDNA, CD-PDMA80-PMPD20/pDNA, and CD-PDMA80-PMPD40/pDNA complexes at weight ratios of 2:1, 16:1, 20:1, and 24:1, respectively, in COS-7 cells upon increasing serum concentration. Results are presented as the mean ± SD, $n = 3$. Asterisks (*) denote significant differences ($P < 0.05$, calculated by two population Student's t test), (a–c) using the transfection efficiency of CD-PDMA80 at each weight ratio as control and (d) the transfection efficiency at 10% serum as control.

One of the serious disadvantages of the cationic vector-mediated systemic gene delivery is the significant inhibition effect to transfection in the presence of serum. To inspect the effect of serum concentration on the transfection efficiency of the CD-polymer/pDNA complexes, we carried out transfection experiments in 30 and 50% serum conditions. The transfection efficiency of PEI25k declined dramatically with the increment of serum concentration, and more obvious differences were observed among the performances of the three CD-polymers at each complex ratio compared to the case of 10% serum (Figure 6b,c). For a better explanation, we focused on the transfection efficiency of the vectors at their optimum complexing ratios in different concentrations of serum (Figure 6d). With increasing serum concentration, the transfection efficiencies of the vectors were affected to a different extent. PEI25k and CD-PDMA80 suffered a 75.2 and 38.4% reduction of efficiency, respectively, at 30% serum compared with 10% serum case, while only 15.8 and 3.7% reductions were observed for CD-PDMA80-PMPD20 and CD-PDMA80-PMPD40, respectively. Further increasing the serum concentration to 50% caused a transfection level decline of as high as 88.3 and 54.3% for PEI25k and CD-PDMA80, respectively, but CD-PDMA80-PMPD20 and CD-PDMA80-PMPD40 exhibited only 21.5 and 6.2% decreases, respectively. It is noteworthy that CD-PDMA80-PMPD40 shows considerable superiority over PEI25k and achieves 13 and 28 times higher transfection efficiencies than PEI25k in the presence of 30 and 50% serum, respectively. These results demonstrate that the copolymerized PMPD blocks can substantially enhance the serum stability of polycation vectors, suggesting that CD-PDMA-PMPD vectors hold promising potential for in vivo applications.

The transfection mediated by PEI25k, CD-PDMA80, and CD-PDMA80-PMPD40 was also evaluated using pEGFP-C1 as the reporter gene in COS-7 cells. The transfected cells were visualized with an inverted fluorescent microscope, and the images for cells treated by different vectors in various serum concentrations are given in Figure 7. Similar results were obtained to the luciferase transfection. CD-PDMA80-PMPD40 was still the most tolerant to serum in mediating GFP transfection in COS-7 cells.

3.7. Cellular Uptake of CD-Polymer/pDNA. In addition to promoting the complex stability in the presence of serum, zwitterionic betaines such as sulfobetaine have been reported to facilitate the cellular uptake.[28,29] It is expected that the introduction of PMPD blocks to CDs would aid in the internalization of CD-polymer/pDNA complexes by cells, thus contributing to the enhancement of transfection efficiency. To confirm this, COS-7 cells were transfected by YOYO-1-labeled pDNA condensed by PEI25k, CD-PDMA80, and CD-PDMA80-PMPD40 at their optimal weight ratios of 2:1, 16:1, and 24:1, respectively, in 10 and 50% serum, and the results were obtained by flow cytometry (Figure 8). It was found that zwitterionic PMPD modification significantly increased the cellular uptake compared with PEI25k control and nonzwitterionic modified CDs. Such an increase in cellular uptake was further amplified at a high serum concentration

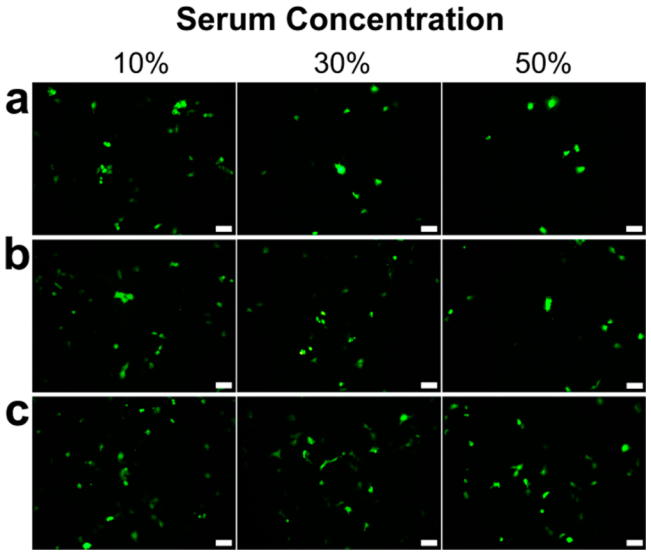

Figure 7. Fluorescent microscope images of COS-7 cells expressing GFP mediated by (a) PEI25k, (b) CD-PDMA80, and (c) CD-PDMA80-PMPD40 (complex ratios were 2:1, 16:1, and 24:1, respectively) at different serum concentrations. Scale bars: 100 μm.

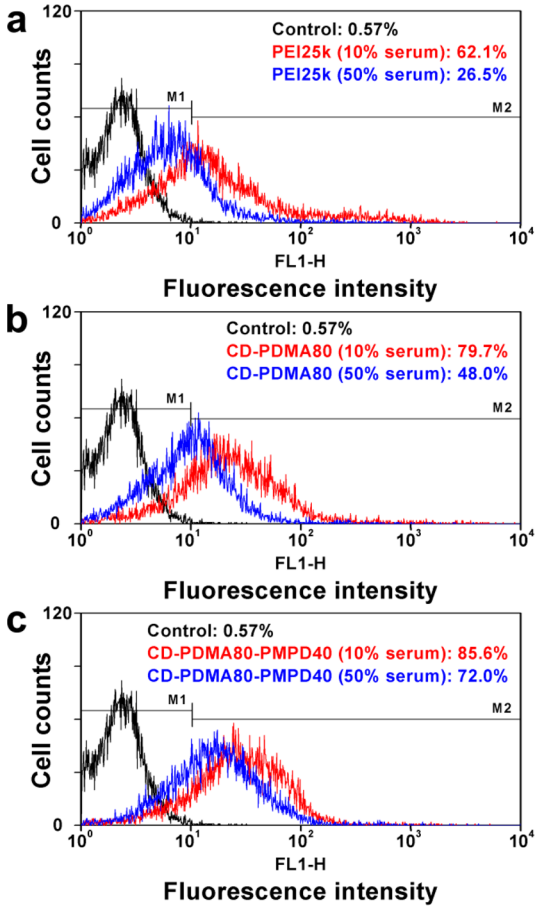

Figure 8. Flow cytometry analysis of (a) cellular uptake of PEI25k/pDNA (2:1 w/w), (b) CD-PDMA80/pDNA (16:1 w/w), and (c) CD-PDMA80-PMPD40/pDNA (24:1 w/w) complexes by COS-7 cells in the presence of 10 and 50% serum concentrations.

(50%). This excellent performance can be attributed to the slightly enhanced hydrophobicity of the polymers after PMPD incorporation, which is beneficial to the enhancement of the interaction between the vectors and cell membrane.[43] The results of cellular uptake further reveal the excellence of introducing PMPD in improving the transfection efficiency of CD-PDMA80.

3.8. Fluorescent Imaging of Nanocomplexes in Living Cells. The polycation/polyzwitterion copolymer grafted CDs in the present study have demonstrated excellent performance in serum-resistant gene delivery. Taking their wavelength-dependent multicolor fluorescence into consideration, they hold the potential to serve as a multifunctional vector with the ability of bioimaging. To confirm this, we chose COS-7 cells for the in vitro transfection and labeling by CD-PDMA80-PMPD40/pDNA complexes. Figure 9 presents the photographs of the as-transfected cells and negative controls taken by a laser scanning confocal microscope. Nearly no fluorescence was detected in control cells, while bright blue, green, and red fluorescence were observed at 405, 488, and 543 nm wavelength laser excitation in the COS-7 cells transfected for 4 h, consistent with the aforementioned fluorescence microscopy assay. Fluorescence was distributed mainly in the cell membrane and the cytoplasm, especially around the cell nucleus, suggesting that the complexes had been successfully internalized into the cells. Remarkably, CD-PDMA80-PMPD40 showed no blinking and low photobleaching under the confocal laser, indicating its good photostability and great potential as bioimaging materials. Moreover, the multicolor emission endows the CD-polymer with more flexibility in biolabeling application, and by changing the excitation wavelength, near-infrared imaging might even be realized.

4. CONCLUSION

In summary, CD-PDMA-PMPD core/shell composites with different polymer block chain lengths were successfully synthesized by surface-initiated ATRP. The obtained CD-polymers were able to condense plasmid DNA into stable nanosized particles and protect DNA from enzymatic degradation. In comparison with CD-PDMA80 and PEI25k, the CD-PDMA-PMPD exhibited lower cytotoxicity, significantly suppressed BSA protein adsorption and superior hemocompatibility. The polycation/polyzwitterion copolymer modified CDs presented a superior serum-tolerant property and an enhanced cellular internalization. PEI25k showed dramatically dropped transfection efficiency upon increasing the serum concentration, while zwitterionic PMPD modified CDs (e.g., CD-PDMA80-PMPD40) maintained the stably high transfection performance, and displayed 13 and 28 times higher transfection efficiencies than PEI25k under 30 and 50% serum, respectively. Fluorescent studies suggested that the photoluminescent attributes, especially the tunable emission property, were well retained after surface modification, and the multicolored fluorescent emissions in transfected cells could be readily detected by laser scanning confocal microscope, suggesting that the CD-polymer hybrid will be a promising platform for serum-resistant gene delivery and imaging. It is anticipated that this new type of multifunctional nanomaterial will pave the way for the development of more CD-based gene theranostic systems. The introduction of ATRP will contribute to the design of future controllable and versatile CD surface coatings and broaden the range of their applications.

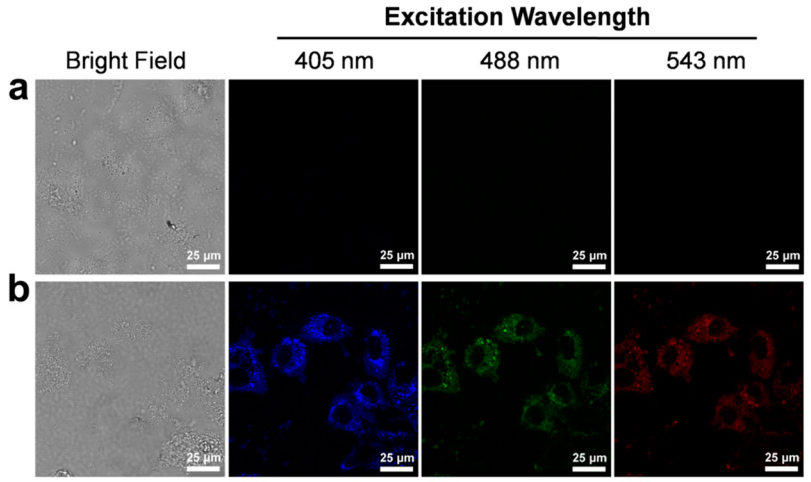

Figure 9. Laser scanning confocal microscopy images of (a) nontransfected COS-7 cells as negative control and (b) CD-PDMA80-PMPD40/pDNA transfected cells. The samples were observed under bright field and excited at 405, 488, and 543 nm. Scale bars: 25 μm.

■ ASSOCIATED CONTENT

Supporting Information

Supplementary experimental section; XRD and Raman spectra of CDs; FTIR and ^{1}H NMR spectra of CDs, CD-Br, and CD-polymers; XPS results of CDs and CD-Br; electrophoresis results of CD-polymers; zeta potential, hydrodynamic size, and TEM images of CD-polymer/pDNA complexes; and MTT assay results of CD-polymer/pDNA complexes, etc. This material is available free of charge via the Internet at http://pubs.acs.org.

■ AUTHOR INFORMATION

Corresponding Author

* E-mail: wgliu@tju.edu.cn.

Author Contributions

§These authors contributed equally.

Notes

The authors declare no competing financial interest.

■ ACKNOWLEDGMENTS

The authors gratefully acknowledge the support for this work from National Science and Technology Major Project of China (Grants 2012ZX10004801-003-007 and 2012AA022603) and the National Natural Science Foundation of China (Grant 51325305).

■ REFERENCES

(1) Doane, T. L.; Burda, C. The Unique Role of Nanoparticles in Nanomedicine: Imaging, Drug Delivery, and Therapy. *Chem. Soc. Rev.* **2012**, *41*, 2885−2911.

(2) Shim, M. S.; Kwon, Y. J. Stimuli-Responsive Polymers and Nanomaterials for Gene Delivery and Imaging Applications. *Adv. Drug Delivery Rev.* **2012**, *64*, 1046−1059.

(3) Baker, S. N.; Baker, G. A. Luminescent Carbon Nanodots: Emergent Nanolights. *Angew. Chem., Int. Ed.* **2010**, *49*, 6726−6744.

(4) Resch-Genger, U.; Grabolle, M.; Cavaliere-Jaricot, S.; Nitschke, R.; Nann, T. Quantum Dots versus Organic Dyes as Fluorescent Labels. *Nat. Methods* **2008**, *5*, 763−775.

(5) Hardman, R. A Toxicologic Review of Quantum Dots: Toxicity Depends on Physicochemical and Environmental Factors. *Environ. Health Perspect.* **2006**, *114*, 165−172.

(6) Yang, S. T.; Wang, X.; Wang, H.; Lu, F.; Luo, P. G.; Cao, L.; Meziani, M. J.; Liu, J. H.; Liu, Y.; Chen, M.; Huang, Y.; Sun, Y. P. Carbon Dots as Nontoxic and High-Performance Fluorescence Imaging Agents. *J. Phys. Chem. C* **2009**, *113*, 18110−18114.

(7) Qian, Z.; Shan, X.; Chai, L.; Ma, J.; Chen, J.; Feng, H. Si-Doped Carbon Quantum Dots: A Facile and General Preparation Strategy, Bioimaging Application, and Multifunctional Sensor. *ACS Appl. Mater. Interfaces* **2014**, *6*, 6797−6805.

(8) Ruan, S.; Wan, J.; Fu, Y.; Han, K.; Li, X.; Chen, J.; Zhang, Q.; Shen, S.; He, Q.; Gao, H. PEGylated Fluorescent Carbon Nanoparticles for Noninvasive Heart Imaging. *Bioconjugate Chem.* **2014**, *25*, 1061−1068.

(9) Kong, B.; Zhu, A.; Ding, C.; Zhao, X.; Li, B.; Tian, Y. Carbon Dot-Based Inorganic-Organic Nanosystem for Two-Photon Imaging and Biosensing of pH Variation in Living Cells and Tissues. *Adv. Mater.* **2012**, *24*, 5844−5848.

(10) Zheng, M.; Xie, Z.; Qu, D.; Li, D.; Du, P.; Jing, X.; Sun, Z. On−Off−On Fluorescent Carbon Dot Nanosensor for Recognition of Chromium (VI) and Ascorbic Acid Based on the Inner Filter Effect. *ACS Appl. Mater. Interfaces* **2013**, *5*, 13242−13247.

(11) Li, H.; He, X.; Kang, Z.; Huang, H.; Liu, Y.; Liu, J.; Lian, S.; Tsang, C. H. A.; Yang, X.; Lee, S. T. Water-Soluble Fluorescent Carbon Quantum Dots and Photocatalyst Design. *Angew. Chem., Int. Ed.* **2010**, *49*, 4430−4434.

(12) Cao, L.; Sahu, S.; Anilkumar, P.; Bunker, C. E.; Xu, J.; Fernando, K. A. S.; Wang, P.; Guliants, E. A.; Tackett, K. N.; Sun, Y. P. Carbon Nanoparticles as Visible-Light Photocatalysts for Efficient CO_2 Conversion and beyond. *J. Am. Chem. Soc.* **2011**, *133*, 4754−4757.

(13) Wang, F.; Chen, Y. H.; Liu, C. Y.; Ma, D. G. White Light-Emitting Devices Based on Carbon Dots' Electroluminescence. *Chem. Commun.* **2011**, *47*, 3502−3504.

(14) Choi, H.; Ko, S. J.; Choi, Y.; Joo, P.; Kim, T.; Lee, B. R.; Jung, J. W.; Choi, H. J.; Cha, M.; Jeong, J. R.; Hwang, I. W.; Song, M. H.; Kim, B. S.; Kim, J. Y. Versatile Surface Plasmon Resonance of Carbon-Dot-Supported Silver Nanoparticles in Polymer Optoelectronic Devices. *Nat. Photonics* **2013**, *7*, 732−738.

(15) Wang, Q.; Huang, X.; Long, Y.; Wang, X.; Zhang, H.; Zhu, R.; Liang, L.; Teng, P.; Zheng, H. Hollow Luminescent Carbon Dots for Drug Delivery. *Carbon* **2013**, *59*, 192−199.

(16) Tang, J.; Kong, B.; Wu, H.; Xu, M.; Wang, Y.; Wang, Y.; Zhao, D.; Zheng, G. Carbon Nanodots Featuring Efficient FRET for Real-Time Monitoring of Drug Delivery and Two-Photon Imaging. *Adv. Mater.* **2013**, *25*, 6569−6574.

(17) Zheng, M.; Liu, S.; Li, J.; Qu, D.; Zhao, H.; Guan, X.; Hu, X.; Xie, Z.; Jing, X.; Sun, Z. Integrating Oxaliplatin with Highly Luminescent Carbon Dots: An Unprecedented Theranostic Agent for Personalized Medicine. *Adv. Mater.* **2014**, *26*, 3554−3560.

(18) Lai, C. W.; Hsiao, Y. H.; Peng, Y. K.; Chou, P. T. Facile Synthesis of Highly Emissive Carbon Dots from Pyrolysis of Glycerol;

Gram Scale Production of Carbon Dots/$mSiO_2$ for Cell Imaging and Drug Release. *J. Mater. Chem.* **2012**, *22*, 14403−14409.
(19) Liu, C.; Zhang, P.; Zhai, X.; Tian, F.; Li, W.; Yang, J.; Liu, Y.; Wang, H.; Wang, W.; Liu, W. Nano-Carrier for Gene Delivery and Bioimaging Based on Carbon Dots with PEI-Passivation Enhanced Fluorescence. *Biomaterials* **2012**, *33*, 3604−3613.
(20) Kim, J.; Park, J.; Kim, H.; Singha, K.; Kim, W. J. Transfection and Intracellular Trafficking Properties of Carbon Dot-Gold Nanoparticle Molecular Assembly Conjugated with PEI-pDNA. *Biomaterials* **2013**, *34*, 7168−7180.
(21) Jäger, M.; Schubert, S.; Ochrimenko, S.; Fischer, D.; Schubert, U. S. Branched and Linear Poly(ethylene imine)-Based Conjugates: Synthetic Modification, Characterization, and Application. *Chem. Soc. Rev.* **2012**, *41*, 4755−4767.
(22) Zhang, Y.; Satterlee, A.; Huang, L. In Vivo Gene Delivery by Nonviral Vectors: Overcoming Hurdles? *Mol. Ther.* **2012**, *20*, 1298−1304.
(23) Piao, J. G.; Ding, S. G.; Yang, L.; Hong, C. Y.; You, Y. Z. Bioreducible Cross-Linked Nanoshell Enhances Gene Transfection of Polycation/DNA Polyplex In Vivo. *Biomacromolecules* **2014**, *15*, 2907−2913.
(24) Deshpande, M. C.; Davies, M. C.; Garnett, M. C.; Williams, P. M.; Armitage, D.; Bailey, L.; Vamvakaki, M.; Armes, S. P.; Stolnik, S. The Effect of Poly(ethylene glycol) Molecular Architecture on Cellular Interaction and Uptake of DNA Complexes. *J. Controlled Release* **2004**, *97*, 143−156.
(25) Guo, X.; Huang, L. Recent Advances in Nonviral Vectors for Gene Delivery. *Acc. Chem. Res.* **2011**, *45*, 971−979.
(26) Ladd, J.; Zhang, Z.; Chen, S.; Hower, J. C.; Jiang, S. Zwitterionic Polymers Exhibiting High Resistance to Nonspecific Protein Adsorption from Human Serum and Plasma. *Biomacromolecules* **2008**, *9*, 1357−1361.
(27) Krause, J. E.; Brault, N. D.; Li, Y.; Xue, H.; Zhou, Y.; Jiang, S. Photoiniferter-Mediated Polymerization of Zwitterionic Carboxybetaine Monomers for Low-Fouling and Functionalizable Surface Coatings. *Macromolecules* **2011**, *44*, 9213−9220.
(28) Dai, F.; Liu, W. Enhanced Gene Transfection and Serum Stability of Polyplexes by PDMAEMA-Polysulfobetaine Diblock Copolymers. *Biomaterials* **2011**, *32*, 628−638.
(29) Xiu, K. M.; Zhao, N. N.; Yang, W. T.; Xu, F. J. Versatile Functionalization of Gene Vectors via Different Types of Zwitterionic Betaine Species for Serum-Tolerant Transfection. *Acta Biomater.* **2013**, *9*, 7439−7448.
(30) Wen, Y.; Zhang, Z.; Li, J. Highly Efficient Multifunctional Supramolecular Gene Carrier System Self-Assembled from Redox-Sensitive and Zwitterionic Polymer Blocks. *Adv. Funct. Mater.* **2014**, *24*, 3874−3884.
(31) Zhai, X.; Zhang, P.; Liu, C.; Bai, T.; Li, W.; Dai, L.; Liu, W. Highly Luminescent Carbon Nanodots by Microwave-Assisted Pyrolysis. *Chem. Commun.* **2012**, *48*, 7955−7957.
(32) Tang, L.; Ji, R.; Cao, X.; Lin, J.; Jiang, H.; Li, X.; Teng, K. S.; Luk, C. M.; Zeng, S.; Hao, J.; Lau, S. P. Deep Ultraviolet Photoluminescence of Water-Soluble Self-Passivated Graphene Quantum Dots. *ACS Nano* **2012**, *6*, 5102−5110.
(33) Liu, J.; He, W.; Zhang, L.; Zhang, Z.; Zhu, J.; Yuan, L.; Chen, H.; Cheng, Z.; Zhu, X. Bifunctional Nanoparticles with Fluorescence and Magnetism via Surface-Initiated AGET ATRP Mediated by an Iron Catalyst. *Langmuir* **2011**, *27*, 12684−12692.
(34) Wang, Z. H.; Li, W. B.; Ma, J.; Tang, G. P.; Yang, W. T.; Xu, F. J. Functionalized Nonionic Dextran Backbones by Atom Transfer Radical Polymerization for Efficient Gene Delivery. *Macromolecules* **2010**, *44*, 230−239.
(35) Pouton, C. W.; Seymour, L. W. Key Issues in Non-Viral Gene Delivery. *Adv. Drug Delivery Rev.* **2001**, *46*, 187−203.
(36) Luo, X. H.; Huang, F. W.; Qin, S. Y.; Wang, H. F.; Feng, J.; Zhang, X. Z.; Zhuo, R. X. A Strategy to Improve Serum-Tolerant Transfection Activity of Polycation Vectors by Surface Hydroxylation. *Biomaterials* **2011**, *32*, 9925−9939.
(37) Risbud, M.; Nabi Saheb, D.; Jog, J.; Bhonde, R. Preparation, Characterization and in Vitro Biocompatibility Evaluation of Poly(butylene terephthalate)/Wollastonite Composites. *Biomaterials* **2001**, *22*, 1591−1597.
(38) Ruan, S.; Zhu, B.; Zhang, H.; Chen, J.; Shen, S.; Qian, J.; He, Q.; Gao, H. A Simple One-Step Method for Preparation of Fluorescent Carbon Nanospheres and the Potential Application in Cell Organelles Imaging. *J. Colloid Interface Sci.* **2014**, *422*, 25−29.
(39) Chandra, S.; Das, P.; Bag, S.; Laha, D.; Pramanik, P. Synthesis, Functionalization, and Bioimaging Applications of Highly Fluorescent Carbon Nanoparticles. *Nanoscale* **2011**, *3*, 1533−1540.
(40) Ruan, S.; Qian, J.; Shen, S.; Zhu, J.; Jiang, X.; He, Q.; Gao, H. A Simple One-Step Method to Prepare Fluorescent Carbon Dots and Their Potential Application in Non-Invasive Glioma Imaging. *Nanoscale* **2014**, *6*, 10040−10047.
(41) Cerda-Cristerna, B. I.; Flores, H.; Pozos-Guillén, A.; Pérez, E.; Sevrin, C.; Grandfils, C. Hemocompatibility Assessment of Poly(2-dimethylamino ethylmethacrylate) (PDMAEMA)-Based Polymers. *J. Controlled Release* **2011**, *153*, 269−277.
(42) Zhang, P.; Yang, J.; Li, W.; Wang, W.; Liu, C.; Griffith, M.; Liu, W. Cationic Polymer Brush Grafted-Nanodiamond via Atom Transfer Radical Polymerization for Enhanced Gene Delivery and Bioimaging. *J. Mater. Chem.* **2011**, *21*, 7755−7764.
(43) Sumerlin, B. S.; Lowe, A. B.; Stroud, P. A.; Zhang, P.; Urban, M. W.; McCormick, C. L. Modification of Gold Surfaces with Water-Soluble (Co) Polymers Prepared via Aqueous Reversible Addition-Fragmentation Chain Transfer (RAFT) Polymerization. *Langmuir* **2003**, *19*, 5559−5562.